Atmos. Chem. Phys. Discuss., 12, 4755–4796, 2012
www.atmos-chem-phys-discuss.net/12/4755/2012/
doi:10.5194/acpd-12-4755-2012

Atmospheric Chemistry and Physics Discussions

Semi-continuous gas and inorganic aerosol measurements at a Finnish urban site: comparisons with filters, nitrogen in aerosol and gas phases, and aerosol acidity

U. Makkonen[1], **A. Virkkula**[1,2], **J. Mäntykenttä**[1], **H. Hakola**[1], **P. Keronen**[2], **V. Vakkari**[2], **and P. P. Aalto**[2]

[1]Finnish Meteorological Institute, 00560, Helsinki, Finland
[2]Department of Physics, University of Helsinki, 00014, Helsinki, Finland

Received: 5 January 2012 – Accepted: 30 January 2012 – Published: 10 February 2012

Correspondence to: A. Virkkula (aki.virkkula@helsinki.fi)

Published by Copernicus Publications on behalf of the European Geosciences Union.

Abstract

Concentrations of 5 gases (HCl, HNO_3, HONO, NH_3, SO_2) and 8 major inorganic ions in particles (Cl^-, NO_3^-, SO_4^{2-}, NH_4^+, Na^+, K^+, Mg^{2+}, Ca^{2+}) were measured with an on-line monitor MARGA 2S in two size ranges, $D_p < 2.5\,\mu m$ and $D_p < 10\,\mu m$, in Helsinki, Finland from November 2009 to May 2010. The results were compared with filter sampling, mass concentrations obtained from particle number size distributions, and a conventional SO_2 monitor. The MARGA yielded lower concentrations than those analyzed from the filter samples for most ions. Linear regression yielded MARGA vs. filter slopes of 0.68, 0.89, 0.84, 0.52, 0.88, 0.17, 2.88, and 3.04 for Cl^-, NO_3^-, SO_4^{2-}, NH_4^+, Na^+, K^+, Mg^{2+}, and Ca^{2+}, respectively, and 0.90 for the MARGA vs. SO_2 monitor. There were clear seasonal cycles in the concentrations of the nitrogen-containing gases: the median concentrations of HNO_3, HONO, and NH_3 were 0.09 ppb, 0.37 ppb, and 0.01 ppb in winter, respectively, and 0.15, 0.15, and 0.14 in spring, respectively. The gas-phase fraction of nitrogen decreased roughly with decreasing temperature so that in the coldest period from January to February the median contribution was 28 % but in April to May 53 %. There were also large fractionation variations that temperature alone cannot explain. HONO correlated well with NO_x but a large fraction of the HONO-to-NO_x ratios were larger than published ratios in a road traffic tunnel suggesting that a large amount of HONO had other sources than vehicle exhaust. Aerosol acidity was estimated by calculating ion equivalent ratios. The sources of acidic aerosols were studied with trajectory statistics that showed that continental aerosol is mainly neutralized and marine aerosol acidic.

1 Introduction

Concentrations of major inorganic ions in aerosols have been measured for decades by sampling on filters and subsequently analyzing them with ion chromatography (e.g. Mulik et al., 1976; Stevens et al., 1978; Mulik and Sawicki, 1979). This kind of

ACPD
12, 4755–4796, 2012

measurements are an integral part of monitoring networks such as the European Monitoring and Evaluation Programme (EMEP) (EMEP, 2007). With filter sampling time resolution is low, from some hours to days, depending on concentrations. In addition, filter sampling suffers from both negative and positive artifacts (e.g. Lipfert, 1994). In order to study atmospheric processes, methods have been developed for measuring aerosol chemical composition at a higher time resolution and to avoid the artifacts associated with filter sampling.

A method with a good time resolution, in the order of seconds/minutes is the Aerosol Mass Spectrometer (AMS) (Jayne et al., 2000; Jimenez et al., 2003) that provides size-resolved chemical composition of submicron aerosols. The AMS measures the concentrations of major aerosol constituents: organics, sulfate, nitrate, ammonium, and chloride. The disadvantage of it is that it does not detect some other important elements such as sodium or calcium that are the main constituents of sea salt and soil dust, respectively. To analyze also them, semicontinuous methods involving ion chromatography have been developed. In these methods sample is first taken for a period of some minutes to hours and then analyzed. An example is the Particle Into Liquid Sampler (PILS) that can be connected for instance to an ion chromatograph (IC) or an instrument for analyzing the concentration of water-soluble organic carbon (Weber et al., 2001; Orsini et al., 2003; Sullivan et al., 2004). The PILS combines two aerosol technologies: particle growth in a mixing condensation particle counter, and droplet collection by a single jet inertial impactor. It takes advantage of the principle of Steam-Jet Aerosol Collector (SJAC) (e.g. Khlystov et al., 1995). Another semicontinuous method that uses a SJAC is the ambient ion monitor (AIM, URG Corporation, USA) that determines the concentrations several anions and cations in aerosol (e.g. Wu and Wang, 2007; Nie et al., 2010), and the Dionex Gas Particle Ion Chromatography (GPIC) system that measures concentrations of water-soluble inorganic aerosol constituents (Cl^-, NO_3^-, SO_4^{2-}, and NH_4^+) and their associated precursor gases (HCl, SO_2, HNO_3, NH_3) (Godri et al., 2009).

ACPD
12, 4755–4796, 2012

The instrument for Measuring AeRosols and GAses (MARGA) (ten Brink et al., 2007) has a SJAC (Slanina et al., 2001) and it is connected to two ion chromatographs, one for anions and another for cations. In addition, it also measures the concentrations of water-soluble gases that produce ions observable with an IC, using the principles presented, e.g. by Wyers et al. (1993). Trebs et al. (2004) used basically the same method, even though they did not call it MARGA then, at a rural site in the Amazon Basin. The instrument consisted of a wet rotating annular denuder in combination with a SJAC followed by an IC for measuring anions and flow injection analysis (FIA) for measuring ammonium, other cations were not measured. The MARGA was used to monitor the size distribution of nitrate, ammonium, sulphate and chloride in aerosol at the top of a meteo-tower of Cabauw (at 200 m) in Netherlands (ten Brink et al., 2007). Four parallel impactors with cut-offs of 0.18, 0.32, 0.56 and 1.0 µm were attached to the MARGA inlet. In a clean background environment a MARGA has been used at an EMEP supersite in Scotland (Cape, 2009).

A commercially available MARGA (Applikon Analytical BV, Netherlands) was operated by the Finnish Meteorological Institute Air Quality Research (FMI/AQR) at the urban background station in Kumpula, Helsinki, from November 2009 to May 2010. These were the first semi-continuous measurements of sulphur dioxide (SO_2), nitric acid (HNO_3), nitrous acid (HNO_2 or HONO), hydrochloric acid (HCl) and ammonia (NH_3) using a rotating wet annular denuder in combination with an on-line ion chromatograph in Finland. In addition, the major anion (Cl^-, NO_3^-, SO_4^{2-}) and cation (NH_4^+, Na^+, K^+, Mg^{2+}, Ca^{2+}) concentrations in aerosols in two size ranges, $D_p < 2.5$ µm ($PM_{2.5}$) and $D_p < 10$ µm (PM_{10}) were measured with the instrument.

The most important goal of this study was to investigate whether the MARGA could be used to replace the traditional EMEP filter pack method (EMEP, 2007). Furthermore, the Clean Air for Europe (CAFE) Directive (EU 2008/50/EC) demands that the member states measure also the chemical composition of $PM_{2.5}$. For monitoring networks it is important that the measurement methods give comparable results. There are published comparisons between filter sampling and semicontinuous methods (e.g.

ACPD
12, 4755–4796, 2012

Nie et al., 2010) but not with the commercially available MARGA. Trebs et al. (2008) compared Amazonian ammonium, nitrate, chloride, and sulphate concentrations analyzed from filter samples with those measured with an instrument similar to MARGA. In the comparison ammonium was the only cation, and in that instrument it was analyzed with FIA. In the instrument used in the present work five cations were analyzed, all with an IC. To our knowledge, there are no published comparisons between a MARGA that analyzes the concentrations of all the above-mentioned three anions and five cations and conventional filter sampling methods.

In this paper the performance of the MARGA 2S instrument is first evaluated by comparing it with independent methods: filter sampling, mass concentrations obtained from particle number size distributions, and a conventional SO_2 monitor. Next the observations on nitrogen compounds both in the gas and aerosol phases are discussed, and finally the aerosol data are used to study aerosol acidity and its sources.

2 Experimental

2.1 Measurement site

The Station for Measuring Ecosystem-Atmosphere Relationships (SMEAR III) is located next to the main building of the Finnish Meteorological Institute (FMI) on a rocky hill 26 m a.s.l., about 5 km northeast of the city center. The station consists of a measurement container and meteorological measurements on ground and in a tower. The container is air conditioned and kept at a constant temperature at 20 °C. A comprehensive description of the SMEAR III station can be found in Järvi et al. (2009).

2.2 MARGA

Concentrations of 5 gases (HCl, HNO_3, HONO, NH_3, SO_2) and 8 major inorganic ions in particles (Cl^-, NO_3^-, SO_4^{2-}, NH_4^+, Na^+, K^+, Mg^{2+}, Ca^{2+}) were measured with

ACPD
12, 4755–4796, 2012

a MARGA 2S from 1 November 2009 to 24 May 2010. The MARGA 2S ADI 2080 (Applikon Analytical BV, The Netherlands) consists of two identical sample boxes and one analytical box. Ambient air was drawn at the flow rate of 1 $m^3 h^{-1}$ into the PM_{10} sample box through a PM_{10}-inlet (Teflon coated, URG-2000-30DBQ) and into the $PM_{2.5}$ sample box through a $PM_{2.5}$ cyclone (1 $m^3 h^{-1}$ Teflon coated inlet, URG-2000-30ENB). However, the first part of the measurements (1 November 2009–19 January 2010) was carried out without a specific inlet, there was just a rain shield on the inlet tubings. The PM_{10}-inlet and the $PM_{2.5}$ cyclone were installed on the 19 January 2010.

Sample air was first drawn through the Wet Rotating Denuder (WRD) where water-soluble gases diffused to the absorption solution, then particles were collected in a Steam Jet Aerosol Collector (SJAC) (Slanina et al., 2001). Diluted hydrogen peroxide solution (10 ppm) was used as the absorption solution to prevent microbiological growth. Absorption solutions were drawn from the WRD and the SJAC to syringes (25 ml) in the analytical box. Each hour after the syringes had been filled, samples were injected to Metrohm anion (250 µl loop) and cation (500 µl loop) chromatographs with the internal standard (LiBr). Cations were separated in a Metrosep C4 (100/4.0) cation column using 32 mmol l^{-1} HNO_3 eluent. For anions a Metrosep A Supp 10 (75/4.0) column and Na_2CO_3 - $NaHCO_3$ (7 mmol l^{-1}/8 mmol l^{-1}) eluent was used. Components were detected by conductivity measurements. For anions a chemical suppressor (H_3PO_4 for regeneration) was used. The detection limits for all the components were 0.1 µg m^{-3} or better, except for K (0.16 µg m^{-3}), Mg (0.12 µg m^{-3}) and Ca (0.21 µg m^{-3}). The detection limits and the repeatability of the instrument studied from the parallel measurements of the two sample boxes (neither the PM_{10}-inlet nor $PM_{2.5}$ cyclone was used) are presented in Table 1.

Field blanks for gases were checked by installing filters in the sampling line before the denuder of the instrument. An oxalic-acid-impregnated filter was used to remove ammonia and a NaOH-impregnated filter to remove acidic gases. The blank values for gases were insignificant, except for nitric acid. The instrument blank for nitrate and nitric acid was remarkable, of the order of 0.4 µg m^{-3} and the blank value caused by

ACPD
12, 4755–4796, 2012

the instrument was subtracted from the results. The high nitrate blank was caused by small amounts of cation eluent leaking continuously to the anion injector.

2.3 Filter sampling

The aerosol results of MARGA were compared with the results of daily sampling of PM_{10} (Digitel PM_{10} sampling inlet, $1\,m^3\,h^{-1}$) and $PM_{2.5}$ (Digitel $PM_{2.5}$ inlet, $1\,m^3\,h^{-1}$) on Teflon filters. The filters were extracted in ultrapure water (Milli-Q) and analysed by ion chromatographs (Waters). The procedure is described in detail in the EMEP Manual (EMEP, 2007). Daily averages were calculated from the MARGA results and compared with the results of the filter method from 5 February to 5 May 2010.

2.4 Other measurements

The routine measurements of the SMEAR III station include particle number size distribution measurements with a Twin DMPS (TDMPS) in the size range 3–950 nm, SO_2 measurements with a Horiba APSA 360 monitor; O_3 measurements with a TEI 49 monitor, and NO_x measurements with a TEI 42S monitor. There is also other instrumentation at the site, see Järvi et al. (2009) for details, but those mentioned above are used here. The number size distributions were used for estimating submicron aerosol mass concentration and comparing that with the sum of the analyzed ions. The SO_2 concentrations could be used as such since the MARGA also measures it. The NO_x and ozone concentrations were used for studies of nitric and nitrous acid.

3 Results and discussion

A statistical summary of the MARGA data is presented in Table 2, including averages, standard deviations, selected percentiles of the cumulative distribution of concentrations, and the fraction of time data is obtained for each ion or gas. When calculating the averages, data values below detection limit were taken into account by giving them

ACPD
12, 4755–4796, 2012

the value of 0.5×(detection limit). The concentrations of sulphate, nitrate, ammonium, and calcium were most of time higher than the detection limits. The lowest fraction of concentrations above detection limit in PM_{10} was for potassium.

The gas-phase concentrations presented below are in ppb and the aerosol concentrations in $\mu g\,m^{-3}$ at 20 °C and 1013 mbar. The time of the measurements in the figures is the local winter time (UTC + 2 h).

3.1 Temporal variations of aerosol concentrations

Several observations can be made already from the time series of the concentrations of the ions analyzed from the aerosol phase in both the $PM_{2.5}$ and PM_{10} size ranges (Fig. 1). The data for which the MARGA software automatic fitting routine to the chromatograms does not yield any concentrations are given as a discontinuity in the graph. This is an effective detection limit. The software does not always recognize a small sodium peak next to a larger ammonium peak or vice versa. Part of the breaks in the time series is due to the fact that the instrument was not running because of some technical issue such as maintenance operations. For chloride there is an additional reason for the discontinuities: before the anion column gets exhausted the chloride peak slowly disappears to the water dip in the beginning of the chromatogram.

The two size ranges measured with the MARGA followed well each other, especially for sulfate, ammonium and nitrate but worse for calcium and magnesium. This is reasonable as it is well known that the latter two are major constituents of soil dust that is in large particles. The size fractions will be discussed more below.

The variation of the aerosol concentrations has two types: short peaks that are probably due to some local source in Helsinki, and slower, several-day-long variations that are due to long-range transport. The latter will be discussed below by using backtrajectories. One interesting peak can be mentioned. The highest potassium concentrations were measured during the New Year Eve celebrations: K^+ concentrations rose above $1\,\mu g\,m^{-3}$ at 19:00 p.m. on 31 December 2009, reached the peak $8.1\,\mu g\,m^{-3}$ at 21–22 and decreased again below $1\,\mu g\,m^{-3}$ at 03:00 a.m. on 1 January 2010. In this same fireworks-related peak also the concentrations of the other ions increased clearly.

ACPD
12, 4755–4796, 2012

The sum of the analyzed ions follows well the temporal variation of the mass concentration calculated from the DMPS (Fig. 2). Here the mass concentration from the DMPS data was calculated assuming the density of 1.5 g cm^{-3}. This figure is shown because it was of interest to see how the MARGA data compares with an independent estimate for aerosol mass concentration. Figure 2 shows that the high and low concentrations with the two methods occurred mainly simultaneously. However, the ion concentrations obviously explain only part of the mass: even if we compare PM_1 from the DMPS and the sum of ions in PM_{10} from the MARGA, PM_1 is 97 % of time larger than the sum of the ions. This means that a large fraction of aerosol mass has not been analyzed. This is in line with earlier studies, for instance by Timonen et al. (2008) who observed that most of aerosol mass often consists of organics also in Helsinki.

3.2 Comparisons of aerosol data with ions analyzed from filter samples

The concentrations measured with the MARGA after the PM_{10} inlet was installed were compared with those analyzed from the Teflon filters by plotting them in the time series (Fig. 1) and by calculating linear regressions (Fig. 3). For the regressions the hourly MARGA data were first averaged over the sampling periods of the filters. In the averaging the values below detection limits were ignored, so that for example if during a selected filter-sampling period there were only four hours when concentrations were above the detection limit, the average is the average of these four hours. The regressions were calculated both within the scatter plots and by using the MS Excel *linest* function. The latter also gives the uncertainties of the slope and offset as standard errors (*stderr*). From these the respective standard deviations were calculated from $stdev = \sqrt{n} \cdot stderr$ where n is the number of observations. For some of the data pairs the two methods give different slopes and offsets. The clearest this is for ammonium and nitrate. In these cases both regression lines are shown in Fig. 3. The slopes, offsets and their uncertainties are given in Table 3.

ACPD
12, 4755–4796, 2012

The MARGA gives lower concentrations for most of the ions even though the averaging method was as explained above. If values below detection limit had been taken into account for instance by giving them values 0.5 × (detection limit) the slopes would have been even lower. From these data alone it is not possible to determine whether the MARGA or the filter sampling results are closer to the true ones. However, the filter sampling method is routine and the laboratory follows strict EMEP protocols (EMEP, 2007) so this suggests that the concentrations given by the MARGA were underestimated. When the regression was calculated with the *linest* function, the slopes for sulphate, ammonium, and nitrate were all close to each other, ranging from 0.84 to 0.89 but in the range from 0.69 to 0.84 when the other regression method was used (Fig. 3). For ammonium it should also be noted that there is the possibility of a positive artifact in the filter samples. After sampling the filters are stored and handled in a laboratory that is clean. If there is ammonia in the laboratory air that reacts with sulphate in the filters and forms ammonium, the resulting ammonium concentrations are higher than they were originally.

Only for Mg^{2+} and Ca^{2+} the slopes were above one, even clearly, 2.88 and 3.04, respectively. A possible explanation is that there was Mg^{2+} and Ca^{2+} contamination in the system. In April and May there was frequently street dust in the air because of brushing the city streets and roads after the winter and the system should have been cleaned more often. In May the Ca^{2+} concentrations were even more clearly too high and these data were discarded from the regression analyses and from Fig. 1. Still, a puzzling thing is that contamination should lead to low correlation coefficients which is not the case for neither Mg^{2+} nor Ca^{2+}: the respective r^2 values were 0.70 and 0.86. For these two ions, on the other hand, there is one more point: the time series (Fig. 1) show that the concentrations analyzed with the MARGA after the $PM_{2.5}$ inlet were not much different from those analyzed from the PM_{10} Teflon filter. One explanation for this would be that the cutoff diameter of the inlet of the filter sampler was lower than 10 µm. This puzzle remains unsolved.

ACPD
12, 4755–4796, 2012

Sulphate concentrations had the best correlation of MARGA vs. filters with $r^2 = 0.98$, the correlation was lower for the rest of the ions. There was no correlation for potassium ($r^2 = 0.1$). This is clearly due to the fact that most of the K^+ concentrations were below the MARGA detection limit: there was not a single 24-h filter-sampling period when all K^+ concentrations of MARGA were above it.

3.3 Aerosol concentration in the two size ranges

The MARGA aerosol data were used for estimating their contribution to the sum of the analyzed ions and for studying their size distribution (Fig. 4). The latter is of course just a very crude estimate of the size distribution, since there were only two size ranges. At each hour the concentrations were summed up and the ratio of each ion to the sum was calculated. On the average, sulphate is responsible for most (50.4 %) of inorganic ion mass after the $PM_{2.5}$ inlet and slightly less (46.4 %) after the PM_{10} inlet. There are cases when sulphate alone contributed more than 80 % to the sum. Nitrate was the second most important ion, as far as aerosol mass is concerned, and there were cases when nitrate contributed more than 50 % to the sum after both inlets.

The $PM_{2.5}$-to-PM_{10} ratio should never be larger than one. For the averages this is the case for all ions but for ammonium and potassium even the 75th percentile of cumulative distribution of the ratio is >1 (Fig. 4). These are cases when concentrations were very low, just above detection limits and the uncertainties were high. Calcium, magnesium, sodium and chloride are major constituents of soil dust and sea salt. For them the $PM_{2.5}$-to-PM_{10} ratio should be clearly <1 and this proves to be the case, most clearly for calcium. For the sum of all ions 97.5 % of the ratios were <1 so in general the size fractionation seems to work in a logical direction. However, more measurements on the large particles with different methods, for example an impactor with sharp cutoffs should be done to find out the true large particle sampling efficiency of the MARGA.

ACPD
12, 4755–4796, 2012

3.4 Temporal variation of the gases and their relationships

The hourly-averaged concentrations of gases measured with the MARGA (HNO_3, HNO_2, NH_3, and SO_2) are presented in Fig. 5. Of these gases sulphur dioxide is the only one that was measured also with an independent method, a TEI 43iTL monitor. These two agreed well, as is seen in the time series, and in the scatter plot (Fig. 6). For the other gases we can only compare our data with values measured at other sites, just to see whether the values are at a reasonable range.

3.4.1 HNO_3 and HNO_2

To get some estimate of the general level of HNO_3 concentrations the data from the SMEAR II station in Hyytiälä in the southwestern part of central Finland were used for comparison. The average HNO_3 concentration (0.16 ppb) of the whole measurement period at SMEAR III was almost the same as the average HNO_3 measured using a EMEP filter pack at SMEAR II (0.15 ppb) in central Finland at the same period (unpublished data, analyzed at FMI/AQR). The yearly average concentration 0.05 ppb measured with MARGA at the EMEP supersite in south-eastern Scotland in 2007 was much lower (Cape, 2009). So, in principle the order of magnitude of the HNO_3 concentrations is reasonable.

A major pathway in the formation of HNO_3 is the reaction $NO_2 + OH^\bullet + M \rightarrow HNO_3 + M$ where the hydroxyl radical $OH^\bullet$ is originated from photochemical reactions. Nitrous acid HNO_2 formed in the reaction $NO + OH^\bullet + M \rightarrow HNO_2 + M$, on the other hand, is dissociated by solar radiation: $HNO_2 + h\nu \rightarrow OH^\bullet + NO$. Ozone is produced in photochemical reactions in sunlight and it is also transported downward from ozone rich air from above during daytime when mixing is efficient. At night it is destroyed when it reacts rapidly with NO according to $NO + O_3 \rightarrow NO_2 + O_2$ and also due to dry deposition. In locations where NO source is large, ozone can be totally destroyed (Finlayson-Pitts and Pitts, 2000). In other words, when there is sunlight, the expected HNO_3 and O_3 concentrations are higher and the HONO concentrations are lower than

ACPD
12, 4755–4796, 2012

in the darkness. This is in agreement with our observations. Concentrations of the gases relevant to the above discussion are presented during a dark period in December (Fig. 7) and a light period in May (Fig. 8), when there is already a clear diurnal cycle. The concentration of nitrate does not follow the temporal variation of nitric acid, since it is transported over long distances.

During the darkest months (November–January) when sunlight was very limited in the northern latitudes the concentration of nitric acid was mostly below 0.1 ppb and stayed stable throughout day and night. In the beginning of February when the amount of daylight increased and there was still snow cover on the ground, the variation of HNO_3 increased and peaks up to 1–1.5 ppb were detected. In March and April the concentrations were varying below 0.5 ppb. In May HNO_3 concentration increased again and peaked up to 1 ppb. In the spring days there is enough light for the photochemical reactions to form OH-radicals which react with NO_2 forming nitric acid. Also the snow cover affects the amount of radiation. The diurnal cycle was calculated both for the winter and for the spring periods. Only the latter is shown because in winter there was no clear daily pattern. In March–May there was a minimum at 07:00–09:00 a.m. and a clear maximum at 12:00–14:00 p.m. (Fig. 9). This is a very similar cycle as that observed at other sites, for instance Melpitz (Acker et al., 2004; Acker and Möller, 2007) and Zürich (Fisseha et al., 2006). In the HNO_3 profile measured in Switzerland in August 2006 (Wolff et al., 2010) the minimum was during the early morning hours and there was a maximum in the afternoon (16:00–17:00 p.m.), about 4 h later than in our spring period in Helsinki. In the afternoon the HNO_3 concentration decreased, due to the photochemical dissociation and probably also the dry deposition (Fisseha et al., 2006). At night concentrations were lower. The day-to-day variation of HNO_3 was large. It is typically removed with rain-out and deposition on surfaces. Precipitation data have not been used for the analysis.

Contrary to nitric acid, the amount HONO in air was higher in winter and decreased in spring. The highest concentrations were measured in December and January. The maximum (4.3 ppb) was measured on 18 December. From the middle of February

ACPD
12, 4755–4796, 2012

HONO concentrations varied below 1 ppb. Between 21 April and 18 May HONO concentration was at the lowest staying below 0.3 ppb. In winter HONO was higher in the daytime and lower at night having a minimum at 04:00–05:00 a.m. In spring concentrations rose in the early mornings reaching the maximum at 07:00–08:00 a.m. and decreased in the afternoons (minimum at 13:00–16:00 p.m., Fig. 9). Also in Switzerland HONO reached the maximum at about 08:00 a.m. and decreased during the day till 05:00 p.m. (Fisseha et al., 2006).

The amount of HONO in air depends on the NO_x concentration. About half of the NO_x emitted from the earth surface annually arises from fossil fuel combustion and the remainder from biomass burning and emissions from soil (Mosier, 2001). There are indications that HONO may be formed heterogeneously from NO_2 on ground or airborne surfaces, for instance aerosol particles, especially soot, or cloud droplets (e.g. Gutzwiller et al., 2002). Positive correlations between NO_x and HONO have been found. Kurtenbach et al. (2001) made extensive investigations of emissions and heterogeneous formation of HONO in a road traffic tunnel and found that the mean HONO-to-NO_x ratio was 0.008 ± 0.001. We have plotted this ratio and the lower and higher values 0.007 and 0.009 as blue lines together with our data (Fig. 10). It is interesting that when a regression line was fit through the data by forcing the offset to zero, the slope is the same as was observed by Kurtenbach et al. (2001), suggesting that at also our site traffic is a major source of HONO. There are not many data points below the line. This means that most of the time there was at least as much HONO as the Kurtenbach et al. (2001) HONO-to-NO_x ratio predicts. On the other hand, a large amount of the data points are clearly above the line, even by an order of magnitude. This suggests that traffic is not the only source of HONO at our site.

3.4.2 Ammonia

As the major base in the atmosphere, ammonia plays a key role for the neutralization of acidic gases and the formation of particulate matter (Asman et al., 1998; Kirkby et al., 2011). Furthermore, the effects of ammonia deposition can lead to eutrophication

ACPD
12, 4755–4796, 2012

and acidification of soils (Ferm, 1998; Erisman et al., 2001; Butterbach-Bahl et al., 2011). The main sources of ammonia (NH_3) are animal waste, ammonification of humus followed by emission from soils, losses of ammonium-containing fertilizers from soils, industrial emissions, oceans, biomass burning and crops (Asman et al., 1998; Seinfeld and Pandis, 1998). About 50 % to 75 % of NH_3 from terrestrial systems is emitted from animal and crop-based agriculture from animal excreta and synthetic fertilizer application (Mosier, 2001). In winter, when land is covered by snow and the sea is frozen it may be expected that the ammonia concentrations are low. The agriculture-related and soil-related sources are strongest in summer, which as such already leads to a seasonal cycle.

This is just what we have observed: in January and February most NH_3 concentrations were below detection limit. After that concentrations rose slightly and as expected later in spring, in April and May highest peaks (1–3 ppb) were detected. Usually ammonia concentrations increase in May, when the agricultural activities start (Ruoho-Airola et. al., 2010).

The additional explanation for the seasonal cycle of ammonia is related to temperature in another way: at warm temperatures at daytime ammonium nitrate particles may volatilize and at cold temperatures the other way round so the reaction $NH_3 + HNO_3$ (g) $\leftrightarrow$ NH_4NO_3 (s) has a temperature-dependent balance. This are also in agreement with our observations: the concentrations of ammonium and nitrate were highest in winter.

3.4.3 SO_2

There was some seasonality in the SO_2 concentrations, with higher concentrations in winter, in January–February. The highest peak (18 ppb) was measured on 20 February. The anthropogenic impact of SO_2 on the environment primarily results from the combustion of sulphur containing fossil fuels in power and heating plants, in industry and in traffic. There was no clear diurnal variation for SO_2 in November-January, but in February–May the concentrations were clearly higher in the daytime than at night. The average SO_2 was about twice as high at noon than at night.

ACPD
12, 4755–4796, 2012

3.4.4 HCl

The hydrochloric acid (HCl) data is the most discontinuous of the gases. Its concentrations were above the detection limit most of February and March, the rest of the time they were mainly below it. The highest peaks up to 0.5–2 ppb were measured in February and March. HCl stayed close to its detection limit in November-January. In spring it had a maximum at noon. HCl may be formed when some acid, for instance sulphuric or nitric acid replaces chloride from sea-salt aerosols. Anthropogenic sources include coal combustion, biomass burning, and waste incineration (Knipping et al., 2003). Now in our data the highest concentrations were observed in February and March when the Baltic Sea is still frozen. This suggests that the source is not sea salt.

3.5 Nitrogen in gas and aerosol phases

The fractionation of nitrogen into gas (excluding NO_x) and aerosol phases was studied by converting the concentrations into ppb units, adding them up $N_{tot} = NO_3^- + NH_4^+ + HNO_3 + HONO + NH_3$, and calculating the contribution of each of them to N_{tot} (Fig. 11). The variation is large but one observation can be made: in the coldest months January and February most nitrogen is in the aerosol phase, the balance turns to the gas phase when temperature increases. The median and the 95 percent range (2.5th to 97.5th percentiles) of the contribution of gas-phase nitrogen $f(N_{gas}) = (HNO_3 + HONO + NH_3)/N_{tot}$ was 28 % (9–70 %) in January–February, and 53 % (11–81 %) in April–May. This is a general trend but large variations from this are also obvious in the time series. It can be observed that the contribution of nitrate is largest in March, which is not in any of the extremes either for temperature or solar radiation. No good explanation could be given.

Nitrate is formed when nitric acid gets into the aerosol phase. The scatter plot of nitric acid vs. nitrate (Fig. 12) shows that there is a weak positive correlation between these two but the correlation is not at all significant ($r^2 = 0.06$). That the nitrate and nitric acid concentration are not well correlated could already be seen in the time series from

ACPD
12, 4755–4796, 2012

winter and summer (Figs. 7 and 8). A probable explanation is that the nitrate observed at the site is long-range transported whereas the nitric acid is from more local sources.

3.6 Aerosol acidity and source area analysis

The aerosol data were next used for studies on the acidity of aerosols. The major acidifying and long-range transported aerosol components are sulphate, ammonium and nitrate. The ion equivalent sum of anions was calculated from

$$SO^{2-}_{4(ekv)} + NO^{-}_{3(ekv)} + Cl^{-}_{ekv} = \frac{m(SO_4)}{48} + \frac{m(NO_3)}{62} + \frac{m(Cl)}{35.5}$$

and that of the cations from

$$NH^{+}_{4(ekv)} + Na^{+}_{(ekv)} + K^{+}_{ekv} + Ca^{2+}_{ekv} + Mg^{2+}_{ekv} = \frac{m(NH_4)}{18} + \frac{m(Na)}{23} + \frac{m(K)}{39} + \frac{m(Ca)}{20} + \frac{m(Mg)}{12.5}$$

where m stands for mass concentration. The ratio of these is <1 for acidic aerosols and >1 for basic. This calculation was done for the PM_{10} particles. The ratio was calculated with and without taking calcium into account because we wanted to see the effect of soil dust. In winter the aerosol is mainly acidic but in March and April basic (Fig. 13, top panel). It is an indication of the well-known urban air quality problem in all Finnish cities in spring: road dust that is brushed from the roads during the spring cleaning.

On the other hand, if the cation-to-anion ratio is calculated using only ammonium, non-seasalt sulfate ($nssSO_4^{2-} = SO_4^{2-} - 0.25 \cdot Na^{+}$, where 0.25 is the sulfate-to-sodium ratio in sea water), and nitrate, the ratio is essentially the same as when using all of the ions (Fig. 13, middle panel), whereas when only ammonium and nss sulfate is used, the ratio is often much higher than one. This means that there is more ammonium than is needed for neutralizing sulfuric acid into ammonium sulphate. Then the rest of ammonium is neutralizing nitrid acid into ammonium nitrate. However, there are long periods when the ratio is <1. To study the origin of the acidic aerosol, the concentration data were combined with backtrajectories.

ACPD
12, 4755–4796, 2012

HYSPLIT4 (HYbrid Single-Particle Lagrangian Integrated Trajectory) trajectories (Draxler and Hess, 1998; Heinzerling, 2004; HYSPLIT-web) were calculated for an arrival height of 100 m with hourly interval, 96 h back in time. The trajectory data were used in a statistical way, presented earlier by Vakkari et al. (2011). At each time step the measured value of the chosen parameter was assigned to the grid cells ($0.5^{\circ} \times 0.5^{\circ}$) along the corresponding back trajectory so that the arrival time of the trajectory was equal to the measurement time. The geometric mean of values accumulated to each grid cell was calculated. The end result is a concentration field that suggests for each cell passed by air masses on the way to the measurement site, whether it contributed to relatively high or low values monitored at the receptor site. In order to ensure the statistical significance of the result, the geometric mean was calculated only if a minimum number of trajectories, set to 10 in this work, crossed a grid cell.

The analysis was done for nss sulfate, ammonium and nitrate. It shows clearly that these ions come from continental Europe (Fig. 14). When it was done for cation-to-anion ratios that were calculated using all ions, the result is far from clear (Fig. 15). This is because calcium comes with soil dust from near-by sources. But when the calculation is done using only ammonium, sulfate, and nitrate, the difference between continental and marine air from the Norwegian Sea becomes obvious: the continental aerosol is neutralized and the marine not.

4 Summary and conclusions

The first deployment of a MARGA instrument in Finland was presented here. Its performance was analyzed by comparing it with independent methods and the data were used to demonstrate some of the possibilities it gives for atmospheric chemistry studies.

The concentrations measured by the MARGA were mainly lower than those measured with standard Teflon filters. The MARGA yielded lower concentrations than those analyzed from the filter samples for most ions. The MARGA vs. filter slopes were 0.68,

ACPD
12, 4755–4796, 2012

0.89, 0.84, 0.52, 0.88, 0.17, 2.88, and 3.04 for Cl^-, NO_3^-, SO_4^{2-}, NH_4^+, Na^+, K^+, Mg^{2+}, and Ca^{2+}, respectively, and 0.90 for the MARGA vs. SO_2 monitor. The reasons for these discrepancies should be found out and corrected. One of the goals with online measurements is to use them to replace filter sampling within the EMEP network. At the present stage this cannot be recommended.

However, the method is promising and it gives very valuable information on both gas and aerosol phases at time resolutions high enough for process studies. For instance, in spring we observed clear diurnal cycles of nitric and nitrous acids that could not have been observed with some impregnated filter method.

There were clear seasonal cycles of the nitrogen containing gases: the median concentrations of HNO_3, HONO, and NH_3 were 0.09 ppb, 0.37 ppb, and 0.01 ppb in winter, respectively, and 0.15, 0.15, and 0.14 in spring, respectively. The HNO_3 and HONO seasonal cycles were driven by the amount of solar radiation: when there was sunlight, the HNO_3 concentrations were higher and the HONO concentrations were lower than in the darkness. This was also the case with the diurnal cycles of the same gases in spring. Comparison with published HONO-to-NO_x ratios from a road traffic tunnel suggests that at our site traffic is a major source of HONO. On the other hand, a large amount of the HONO-to-NO_x ratios were clearly larger than them, even by an order of magnitude. This shows that traffic is not the only source of HONO at our site.

The seasonal cycle of ammonia was such that in the coldest months the concentrations were mainly below the detection limit and they increased with increasing temperature. This can be explained by agriculture-related and soil-related sources that are low when land is frozen and covered with snow.

The fractionation of nitrogen into gas and aerosol phases was studied by converting all concentrations into ppb units, summing then up and calculating the contribution of each of them to the sum. The gas-phase fraction of nitrogen decreased roughly with decreasing temperature so that in the coldest period from January to February the median contribution was 28 % but in April to May 53 %. However, in all months there were large fractionation variations that temperature alone cannot explain.

ACPD
12, 4755–4796, 2012

The analysis of ion balances showed that in winter aerosol is mainly acidic. In spring it gets basic due to soil dust. The trajectory statistics shows that even though the measurement site is in Helsinki and in the middle of the most densely populated parts of Finland, clear differences can be seen in the degree of neutralization as a function of source area. The long-range transported aerosol is acidic when it comes from the northern sectors and neutralized by ammonia when it comes from Central and Eastern Europe.

Acknowledgements. This work was supported by the Academy of Finland as part or the Centre of Excellence program (project no. 1118615).

References

Acker, K. and Möller, D.: Atmospheric variation of nitrous acid at different sites in Europe, Environ. Chem., 4, 242–255, doi:10.1071/EN07023, 2007.

Acker, K., Spindler, G., and Brüggemann, E.: Nitrous and nitric acid measurements during the INTERCOMP2000 campaign in Melpitz, Atmos. Environ., 38, 6497–6505, doi:10.1016/j.atmosenv.2004.08.030, 2004.

Asman, W. A. H., Sutton, M. A., and Schjørring, J. K.: Ammonia: emission, atmospheric transport and deposition, New Phytol. 139, 27–48, doi: 10.1046/j.1469-8137.1998.00180.x, 1998.

Butterbach-Bahl, K., Gundersen, P., Ambus, P., Augustin, J., Beier, C., Boeckx, P., Dannenmann, M., Gimeno, B. S., Ibrom, A., Kiese, R., Kitzler, B., Rees, R. M., Smith, K. A., Stevens, C., Vesala, T., and Zechmeister-Boltenstern, S.: Nitrogen processes in terrestrial ecosystems, in: The European Nitrogen Assessment, edited by: Sutton, M. A., Howard C. M., Erisman, J. W., Billen, G., Bleeker, A., Grennfelt, P., van Grinsven, H., and Grizzetti, B., Cambridge University Press, Cambridge Books Online, 13 December 2011, doi:10.1017/CBO9780511976988.009, 2011.

Cape, J. N.: Operation of EMEP "supersites" in the United Kingdom, Annual report for 2007, ISBN 978-1-906698-15-7, http://nora.nerc.ac.uk/8660/2/EMEP_supersite_report_2007N008660CR.pdf, 2009.

Draxler, R. and Hess, G.: An Overview of the HYSPLIT_4 modelling system for trajectories,

ACPD

12, 4755–4796, 2012

dispersion and deposition, Aust. Met. Mag., 47, 295–308, http://www.bom.gov.au/amoj/docs/1998/draxler.pdf, 1998.
EMEP manual for sampling and chemical analysis, Norwegian Institute for Air Research, Kjeller, EMEP/CCC-Report 1/95, Rev. 2007, http://www.nilu.no/projects/ccc/manual/index.html, 2007.
Erisman, J. W., Otjes, R., Hensen, A., Jongejan, P., van den Bulk, P., Khlystov, A., Mols, H., and Slanina, J.: Instrument development and application in studies and monitoring of ambient ammonia, Atmos. Environ., 35, 1913–1922, doi:10.1016/S1352-2310(00)00544-6, 2001.
EU 2008/50/EC: Directive 2008/50/EC of the European Parliament and of the Council of 21 May 2008 on ambient air quality and cleaner air for Europe, http://eur-lex.europa.eu/LexUriServ/LexUriServ.do?uri=CELEX:32008L0050:EN:NOT, 2008.
Ferm, M.: Atmospheric ammonia and ammonium transport in Europe and critical loads – A review, Nutrient Cycling in Agroecosystems 51, 5–17, doi:10.1023/A:1009780030477, 1998.
Finlayson-Pitts, B. J. and Pitts, J. N.: Chemistry of the upper and lower atmosphere: theory, experiments and application, Academic Press, San Diego, CA (ISBN 0-12-257060-x), 2000.
Fisseha, R., Dommen, J., Gutzwiller, L., Weingartner, E., Gysel, M., Emmenegger, C., Kalberer, M., and Baltensperger, U.: Seasonal and diurnal characteristics of water soluble inorganic compounds in the gas and aerosol phase in the Zurich area, Atmos. Chem. Phys., 6, 1895–1904, doi:10.5194/acp-6-1895-2006, 2006.
Godri, K. J., Evans, G. J., Slowik, J., Knox, A., Abbatt, J., Brook, J., Dann, T., and Dabek-Zlotorzynska, E.: Evaluation and application of a semi-continuous chemical characterization system for water soluble inorganic PM2.5 and associated precursor gases, Atmos. Meas. Tech., 2, 65–80, doi:10.5194/amt-2-65-2009, 2009.
Gutzwiller, L., Arens, F., Baltensperger, U., Gäggeler, H. W., and Ammann, M.: Significance of Semivolatile Diesel Exhaust Organics for Secondary HONO Formation, Environ. Sci. Technol., 36, 677–682, doi:10.1021/es015673b, 2002.
Heinzerling, D.: Automation of HYSPLIT trajectory generation and subsequent analysis, Washington university, Research for Undergraduates Program 2004, HYSPLIT-web, ARL Air Resources Laboratory: HYSPLIT – Hybrid Single Particle Lagrangian Integrated Trajectory Model, http://ready.arl.noaa.gov/HYSPLIT.php, 2004.
Järvi, L., Hannuniemi, H., Hussein, T., Junninen, H., Aalto, P. P., Hillamo, R., Mäkelä, T., Keronen, P., Siivola, E., Vesala, T., and Kulmala, M.: The urban measurement station SMEAR III: Continuous monitoring of air pollution and surface-atmosphere interactions in Helsinki,

ACPD
12, 4755–4796, 2012

Finland, Boreal Environ. Res., 14, 86–109, 2009.
Jayne, J. T., Leard, D. C., Zhang, X., Davidovits, P., Smith, K. A., Kolb, C. E., and Worsnop, D. R.: Development of an aerosol mass spectrometer for size and composition analysis of submicron particles, Aerosol Sci. Technol., 33, 49–70, 2000.
Jimenez, J. L., Jayne, J. T., Shi, Q., Kolb, C. E., Worsnop, D. R., Yourshaw, I., Seinfeld, J. H., Flagan, R. C., Zhang, X., Smith, K. A., Morris, J. W., and Davidovits, P,: Ambient aerosol sampling using the Aerodyne Aerosol Mass Spectrometer, J. Geophys Res., 108, 8425, doi:10.1029/2001JD001213, 2003.
Khlystov, A., Wyers, G. P., and Slanina, J.: The Steam-Jet Aerosol Collector, Atmos. Environ., 29, 2229–2234, 1995.
Kirkby, J., Curtius, J., Almeida, J., Dunne, E., Duplissy, J., Ehrhart, S., Franchin, A., Gagné, S., Ickes, L., Kürten A., Kupc, A., Metzger, A., Riccobono, F., Rondo, L., Schobesberger, S., Tsagkogeorgas, G., Wimmer, D., Amorim, A., Bianchi, F., Breitenlechner, M., David, A., Dommen, J., Downard, A., Ehn, M., Flagan, R.C., Haider, S., Hansel, A., Hauser, D., Jud, W., Junninen, H., Kreissl, F., Kvashin, A., Laaksonen, A., Lehtipalo, K., Lima, J., Lovejoy, E. R., Makhmutov, V., Mathot, S., Mikkilä, J., Minginette, P., Mogo, S., Nieminen, T., Onnela, A., Pereira, P., Petäjä, T., Schnitzhofer, R., Seinfeld, J. H., Sipilä, M., Stozhkov, Y., Stratmann, F., Tomé A., Vanhanen, J., Viisanen, Y., Vrtala,A., Wagner, P. E., Walther, H., Weingartner, E., Wex, H., Winkler, P. M., Carslaw, K. S., Worsnop, D. R., Baltensperger, U., and Kulmala, M.: Role of sulphuric acid, ammonia and galactic cosmic rays in atmospheric aerosol nucleation, Nature 476, 429–433, doi:10.1038/nature10343, 2011.
Knipping, E. and Dabdub, D.: Impact of Chlorine Emissions from Sea-Salt Aerosol on Coastal Urban Ozone, Environ. Sci. Technol., 37, 275–284, doi:10.1021/es025793z, 2003.
Kurtenbach, R., Becker, K. H., Gomes, J. A. G., Kleffmann, J., Lorzer, J. C., Spittler, M., Wiesen, P., Ackermann, R., Geyer, A., and Platt, U.: Investigations of emissions and heterogeneous formation of HONO in a road traffic tunnel, Atmos. Environ., 35, 3385–3394, doi:10.1016/S1352-2310(01)00138-8, 2001.
Lipfert, F. W.: Filter Artifacts Associated with Particulate Measurements – Recent-Evidence and Effects on Statistical Relationships, Atmos. Environ., 28, 3233–3249, 1994.
Mosier, A. R.: Exchange of gaseous nitrogen compounds between agricultural systems and the atmosphere, Plant and Soil, 228, 17–27, doi:10.1023/A:1004821205442, 2001.
Mulik, J. and Sawicki, E.: Ion chromatography, Environ. Sci. Technol., 13, 804–809, doi:10.1021/es60155a014, 1979.

ACPD
12, 4755–4796, 2012

Mulik, J., Puckett, R., Williams, D., and Sawicki, E.: Ion chromatographic analysis of sulfate and nitrate in ambient aerosols, Anal. Lett., 9, 653–663, doi:10.1080/00032717608059128, 1976.

Nie, W., Wang, T., Gao, X., Pathak, R. K., Wang, X., Gao, R., Zhang, Q., Yang, L., and Wang, W. X.: Comparison among filter-based, impactor-based and continuous techniques for measuring atmospheric fine sulfate and nitrate, Atmos. Environ., 44, 4396–4403, doi:10.1016/j.atmosenv.2010.07.047, 2010.

Orsini, D., Ma, Y., Sullivan, A., Sierau, B., Baumann, K., and Weber, R.: Refinements to the Particle-Into-Liquid Sampler (PILS) for Ground and Airborne Measurements of Water Soluble Aerosol Composition, Atmos. Environ., 37, 1243–1259, doi:10.1016/S1352-2310(02)01015-4, 2003.

Ruoho-Airola, T., Leppänen, S., and Makkonen, U.: Changes in the concentration of reduced nitrogen in the air in Finland between 1990 and 2007, Boreal Environ. Res., 15, 427–436, 2010.

Seinfeld, J. H. and Pandis, S. N.: Atmospheric Chemistry and Physics: From Air Pollution to Climate Change, J. Wiley, New York, 1998.

Slanina, J., ten Brink, H. M., Otjes, R. P., Even, A., Jongejan, P., Khlystov, S., Waijers-Ijpelaan, A., Hu, M., and Lu, Y.: The continuous analysis of nitrate and ammonium in aerosols by the steam jet aerosol collector (SJAC): extension and validation of the methodology, Atmos. Environ., 35, 2319–2330, doi:10.1016/S1352-2310(00)00556-2, 2001.

Sullivan, A. P., Weber, R. J., Clements, A. L., Turner, J. R., Bae, M. S., and Schauer, J. J.: A method for on-line measurement of watersoluble organic carbon in ambient aerosol particles: Results from an urban site, Geophys. Res. Lett., 31, L13105, doi:10.1029/2004GL019681, 2004.

Stevens, R. K., Dzubay, T. G., Russwurm, G., and Rickel D.: Sampling and analysis of atmospheric sulfates and related species, Atmos. Environ., 12, 55–68, doi:10.1016/0004-6981(78)90188-9, 1978.

ten Brink, H. M., Otjes, R., Jongejan, P., and Slanina, J.: An instrument for semi-continuous monitoring of the size-distribution of ammonium nitrate aerosol, Atmos. Environ., 41, 2768–2779, doi:10.1016/j.atmosenv.2006.11.041, 2007.

Timonen, H., Saarikoski, S., Tolonen-Kivimäki, O., Aurela, M., Saarnio, K., Petäjä, T., Aalto, P. P., Kulmala, M., Pakkanen, T., and Hillamo, R.: Size distributions, sources and source areas of water-soluble organic carbon in urban background air, Atmos. Chem. Phys., 8, 5635–5647,

ACPD
12, 4755–4796, 2012

doi:10.5194/acp-8-5635-2008, 2008.
Trebs, I., Meixner, F. X., Slanina, J., Otjes, R., Jongejan, P., and Andreae, M. O.: Real-time measurements of ammonia, acidic trace gases and water-soluble inorganic aerosol species at a rural site in the Amazon Basin, Atmos. Chem. Phys., 4, 967–987, doi:10.5194/acp-4-967-2004, 2004.
Trebs, I., Andreae, M. O., Elbert, W., Mayol-Bracero, O. L., Soto-García, L. L., Rudich, Y., Falkovich, A. H., Maenhaut, W., Artaxo, P., Otjes, R., and Slanina J.: Aerosol inorganic composition at a tropical site: discrepancies between filter-based sampling and a semi-continuous method, Aerosol Sci. Technol., 4, 255–269, doi:10.1080/02786820801992899, 2008.
Vakkari, V., Laakso, H., Kulmala, M., Laaksonen, A., Mabaso, D., Molefe, M., Kgabi, N., and Laakso, L.: New particle formation events in semi-clean South African savannah, Atmos. Chem. Phys., 11, 3333–3346, doi:10.5194/acp-11-3333-2011, 2011.
Weber, R. J., Orsini, D., Daun, Y., Lee, Y.-N., Klotz, P. J., and Brechtel, F.: A Particle into-Liquid Collector for Rapid Measurement of Aerosol Bulk Chemical Composition, Aerosol Sci. Technol., 35, 718–727, doi:10.1080/02786820152546761, 2001.
Wolff, V., Trebs, I., Ammann, C., and Meixner, F. X.: Aerodynamic gradient measurements of the NH_3-HNO_3-NH_4NO_3 triad using a wet chemical instrument: an analysis of precision requirements and flux errors, Atmos. Meas. Tech., 3, 187–208, doi:10.5194/amt-3-187-2010, 2010.
Wu, W. S. and Wang, T.: On the performance of a semi-continuous $PM_{2.5}$ sulphate and nitrate instrument under high loadings of particulate and sulphur dioxide, Atmos. Environ., 41, 5442–5451, 2007.
Wyers, G. P., Otjes, R. P., and Slanina, J.: A continuous flow denuder for the measurement of ambient concentrations and surface fluxes of NH3, Atmos. Environ., 27A, 2085–2090, doi:10.1016/0960-1686(93)90280-C, 1993.

ACPD
12, 4755–4796, 2012

Table 1. The detection limits and the repeatability calculated from real air samples collected using the two parallel sample boxes of the MARGA instrument (1 November 2009–18 January 2010).

Compound	Detection limit $\mu g\,m^{-3}$	Repeatability %
HCl	0.02	30
HNO_2	0.03	3.3
SO_2	0.04	4.9
HNO_3	0.05	1.1
NH_3	0.05	3.9
Cl^-	0.02	4.5
NO_3^-	0.04	1.0
SO_4^{2-}	0.03	1.1
Na^+	0.02	1.2
NH_4^+	0.03	1.9
K^+	0.01	13.3
Mg^{2+}	0.01	8.7
Ca^{2+}	0.01	1.1

ACPD
12, 4755–4796, 2012

Table 2. Statistical summary of the MARGA data measured at SMEAR III station in Helsinki in winter (1 November 2009–28 February 2010) and in spring (1 March–25 May 2010). Five first columns: concentrations of gases in ppb and of aerosols in the two size fractions in $\mu g\,m^{-3}$ at 20 °C, 1013 mbar; N/N_{tot}: fraction of total number of hours during which there is data for the compound; N/N_{tot} ($C > DL$): fraction of total number of hours during which concentration was above detection limit. The winter $PM_{2.5}$ statistics were calculated for the period 19 January–28 February. In winter $N_{tot} = 2879$ for PM_{10} and 919 for $PM_{2.5}$; in spring $N_{tot} = 2047$ for both $PM_{2.5}$ and PM_{10}.

		WINTER						SPRING					
			Percentiles						Percentiles				
		AVE±STD	2.5	50	97.5	N/N_{tot}	N/N_{tot} ($C > DL$)	AVE±STD	2.5	50	97.5	N/N_{tot}	N/N_{tot} ($C > DL$)
HNO_3		0.13±0.12	0.03	0.09	0.38	90 %	90 %	0.22±0.19	0.06	0.15	0.72	85 %	85 %
HNO_2		0.45±0.33	0.11	0.37	1.18	91 %	91 %	0.19±0.14	0.04	0.15	0.64	84 %	84 %
NH_3		0.25±0.44	0.01	0.01	1.33	92 %	92 %	0.28±0.41	0.01	0.14	1.61	85 %	85 %
SO_2		1.32±1.73	0.10	0.65	6.54	92 %	92 %	0.76±1.00	0.11	0.47	3.38	85 %	85 %
HCl		0.03±0.08	n.d.	n.d.	0.18	84 %	36 %	0.04±0.11	n.d.	0.00	0.25	85 %	29 %
Cl^-	$PM_{2.5}$	0.10±0.25	n.d.	0.03	0.62	96 %	56 %	0.04±0.14	n.d.	0.01	0.28	85 %	17 %
	PM_{10}	0.11±0.26	n.d.	0.02	0.73	84 %	45 %	0.08±0.23	n.d.	0.01	0.59	85 %	25 %
NO_3^-	$PM_{2.5}$	2.27±1.76	0.23	1.87	7.41	96 %	95 %	1.40±2.04	0.14	0.68	7.34	84 %	84 %
	PM_{10}	1.50±1.45	0.15	1.09	5.58	91 %	91 %	1.63±2.24	0.18	0.89	8.27	84 %	84 %
SO_4^{2-}	$PM_{2.5}$	3.18±1.23	1.39	2.93	5.78	96 %	96 %	1.64±1.08	0.37	1.45	4.39	84 %	84 %
	PM_{10}	2.15±1.38	0.43	1.76	5.70	92 %	92 %	1.79±1.24	0.41	1.53	4.88	85 %	85 %
Na^+	$PM_{2.5}$	0.05±0.08	n.d.	0.02	0.30	96 %	50 %	0.04±0.11	n.d.	0.01	0.40	80 %	17 %
	PM_{10}	0.08±0.17	n.d.	0.03	0.57	92 %	50 %	0.07±0.18	n.d.	0.01	0.57	80 %	26 %
NH_4^+	$PM_{2.5}$	0.74±0.65	n.d.	0.59	2.55	96 %	93 %	0.46±0.80	n.d.	0.19	2.71	85 %	70 %
	PM_{10}	0.55±0.54	n.d.	0.41	1.95	92 %	84 %	0.49±0.86	n.d.	0.20	2.90	84 %	71 %
K^+	$PM_{2.5}$	0.04±0.07	n.d.	n.d.	0.23	96 %	24 %	0.01±0.04	n.d.	0.01	0.14	80 %	7 %
	PM_{10}	0.06±0.29	n.d.	n.d.	0.27	91 %	27 %	0.02±0.03	n.d.	0.01	0.14	80 %	7 %
Mg^{2+}	$PM_{2.5}$	0.04±0.06	n.d.	0.03	0.19	96 %	51 %	0.05±0.07	n.d.	0.02	0.22	84 %	45 %
	PM_{10}	0.05±0.10	n.d.	0.02	0.24	92 %	50 %	0.09±0.11	n.d.	0.06	0.35	84 %	57 %
Ca^{2+}	$PM_{2.5}$	0.26±0.21	0.07	0.22	0.65	96 %	96 %	0.18±0.24	0.01	0.13	0.72	84 %	84 %
	PM_{10}	0.30±0.26	0.04	0.23	0.96	92 %	91 %	0.50±0.71	0.01	0.26	2.42	83 %	83 %

ACPD
12, 4755–4796, 2012

Table 3. Coefficients of the linear regressions of the concentrations measured with the MARGA data vs. those analyzed from the PM_{10} filters and the SO_2 measured with a Horiba APSA 360 monitor: C(MARGA) = $k \times C$(comparison method) + C_0. The linear regressions were calculated with the MS Excel *linest* function. N = number of observations used in the regression. For explanation of the uncertainties of k and C_0 see Sect. 3.2.

	N	$k \pm$ std(k)	$C_0 \pm$ std(C_0)	r^2
Cl^-	58	0.68 ± 0.33	0.07 ± 0.10	0.81
NO_3^-	87	0.89 ± 0.28	0.51 ± 0.78	0.91
SO_4^{2-}	87	0.84 ± 0.13	0.24 ± 0.31	0.98
Na^+	73	0.52 ± 0.60	−0.01 ± 0.20	0.43
NH_4^+	85	0.88 ± 0.41	−0.25 ± 0.49	0.83
K^+	42	0.17 ± 0.56	0.07 ± 0.07	0.09
Mg^{2+}	87	2.88 ± 1.93	−0.01 ± 0.08	0.70
Ca^{2+}	83	3.04 ± 1.26	0.09 ± 0.22	0.86
SO_2	3701	0.90 ± 0.31	−0.08 ± 0.68	0.89

ACPD
12, 4755–4796, 2012

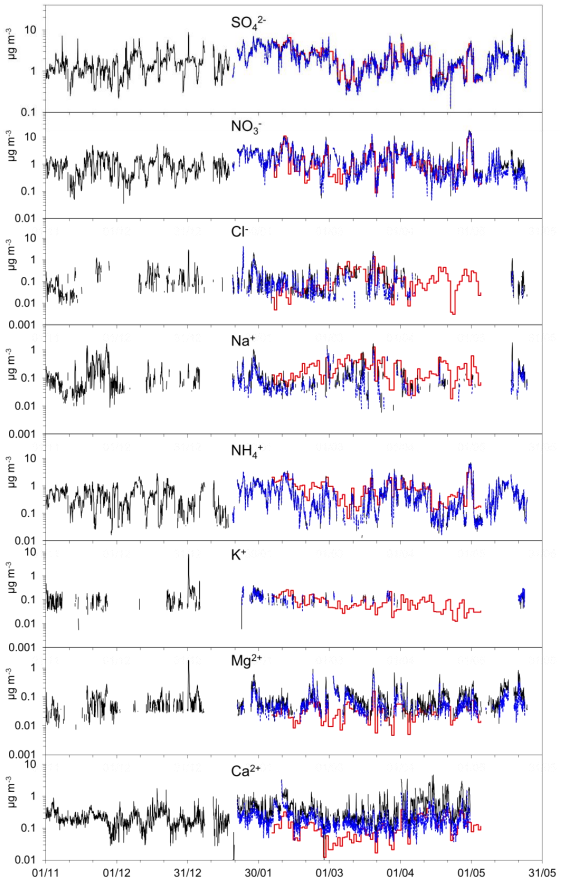

Fig. 1. Hourly-averaged concentrations of inorganic ions in aerosols at SMEAR III from 1 November 2009 to 25 May 2010. MARGA data in PM_{10} (black line) and $PM_{2.5}$ (blue line); concentrations analyzed from 24-h PM_{10} filter samples (red line). Note: before 19 January 2010 there was only a total aerosol inlet in use and no $PM_{2.5}$ cyclone.

ACPD
12, 4755–4796, 2012

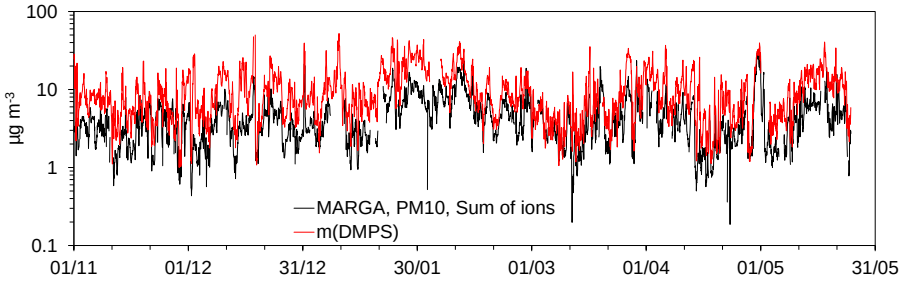

Fig. 2. Sum of inorganic ion concentrations in aerosols measured with MARGA in the size range $D_p < 10$ µm (noting that before 19 January 2010 there was only a total aerosol inlet in use) and the mass concentration of particles estimated from the particle number size distributions (m(DMPS)) in the size range $D_p < 1$ µm and assuming the density of 1.5 g cm^{-3}.

ACPD
12, 4755–4796, 2012

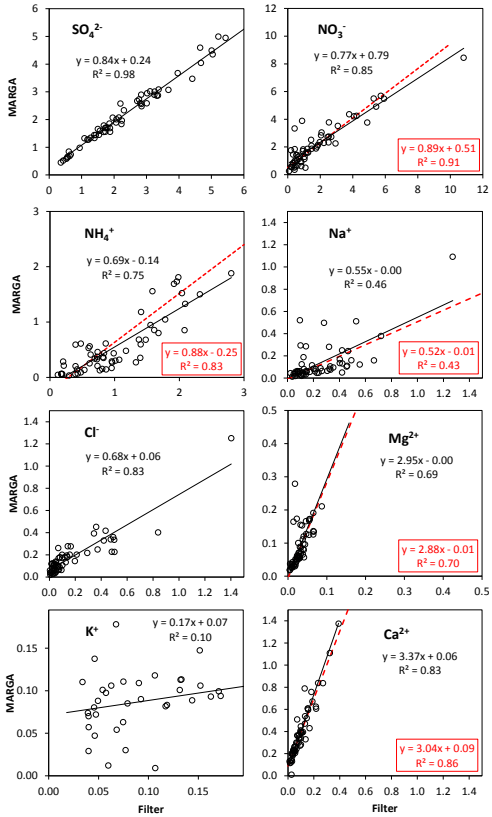

Fig. 3. Comparisons of concentrations of ions in the size range $D_p < 10\,\mu m$ measured with the MARGA and analyzed from Teflon filters. The MARGA data were averaged over the filter sampling periods. Unit: $\mu g\,m^{-3}$. The linear regressions with the black lines and equations were calculated using the fitting routine within the scatter plots and those with the red dashed lines and red equations by using the *linest* function of MS Excel.

ACPD
12, 4755–4796, 2012

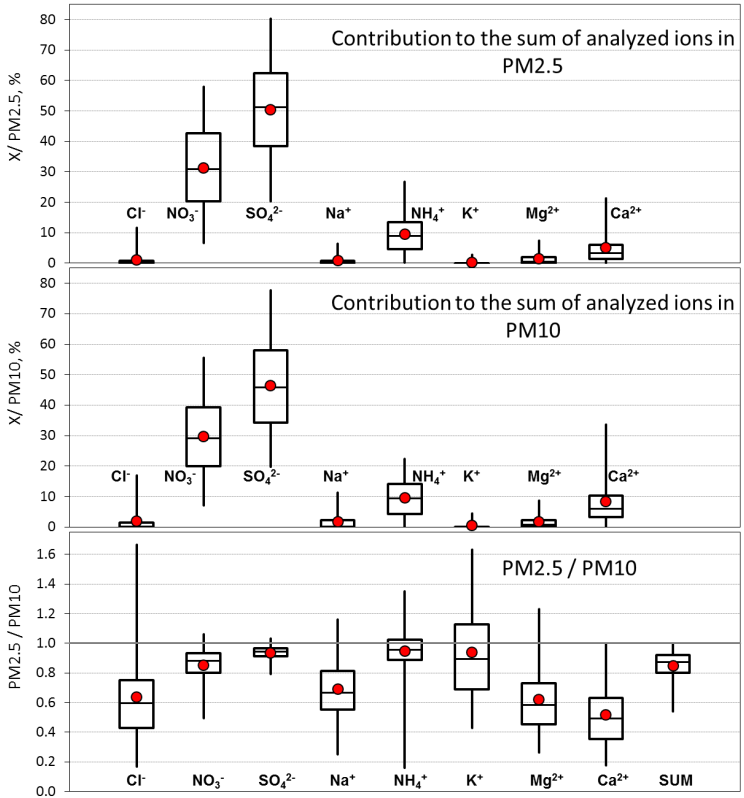

Fig. 4. Contributions of the major ions to their sum and the ratios of ion concentrations analyzed from the two inlets, $PM_{2.5}$ and PM_{10}. The box represents the 25th to 75th percentile range, the bars the 95 percent range (2.5th and 97.5th percentiles), the horizontal line the median and the red circle the averages of the hourly-averaged data.

ACPD
12, 4755–4796, 2012

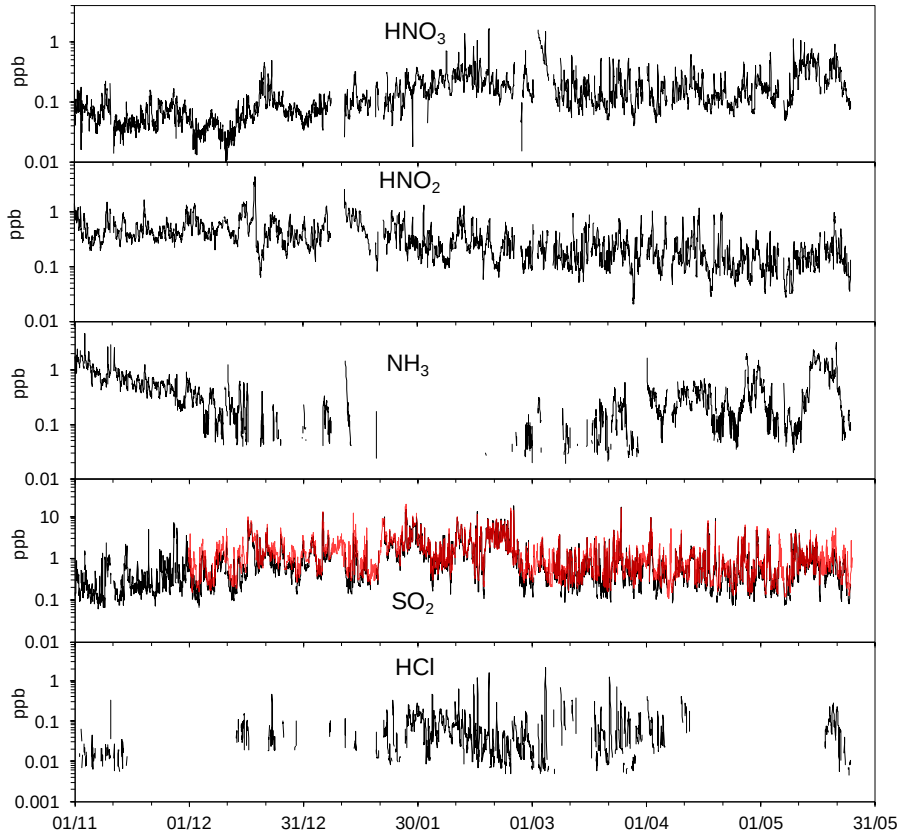

Fig. 5. Hourly-averaged concentrations of gases measured with the MARGA (HNO_3, HNO_2, NH_3, and SO_2) at SMEAR III from 1 November 2009 to 25 May 2010. The red line in the SO_2 time series is the data measured with a TEI 43iTL monitor.

ACPD
12, 4755–4796, 2012

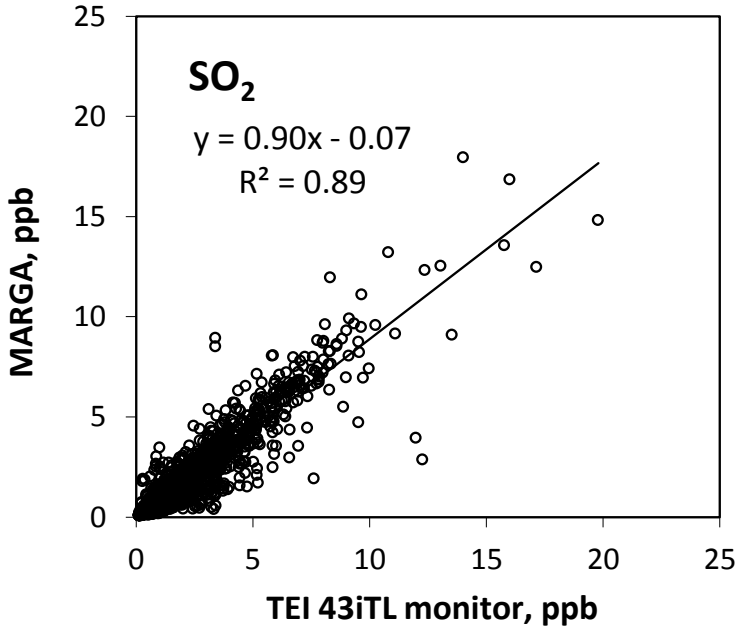

Fig. 6. Sulphur dioxide measured with the MARGA and a TEI 43iTL SO_2 monitor, all hourly averages.

ACPD
12, 4755–4796, 2012

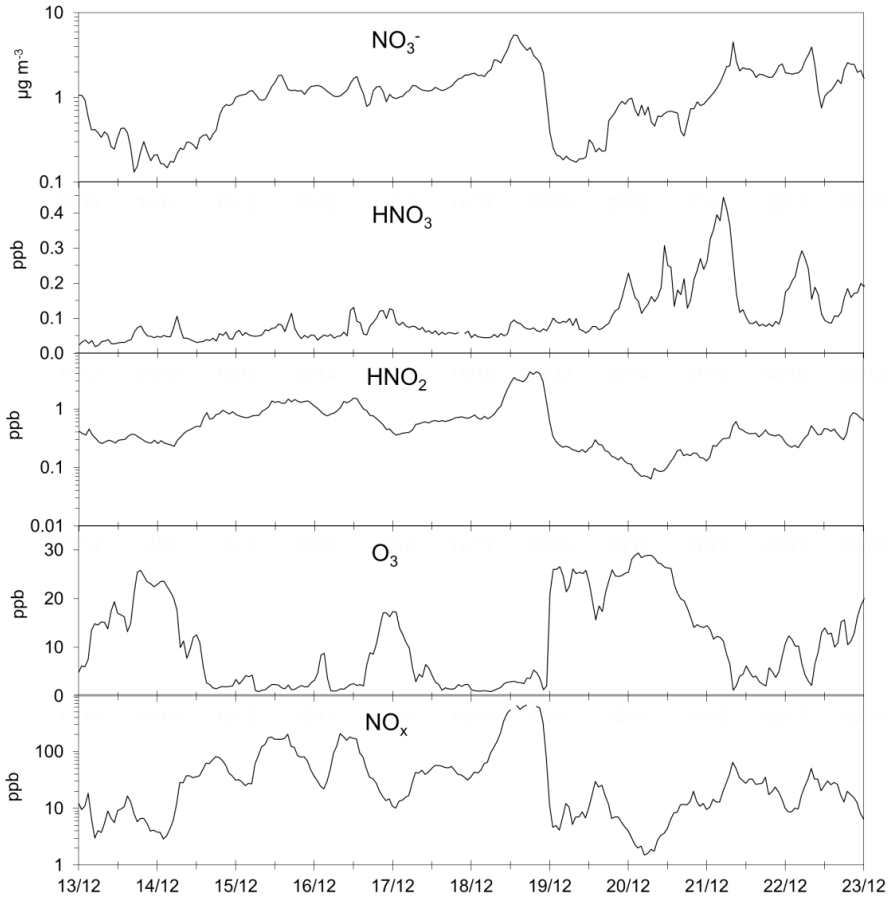

Fig. 7. Ozone, NO_x, and the nitrogen-containing gas-phase acids and nitrate in PM_{10} in the dark time of the year.

ACPD
12, 4755–4796, 2012

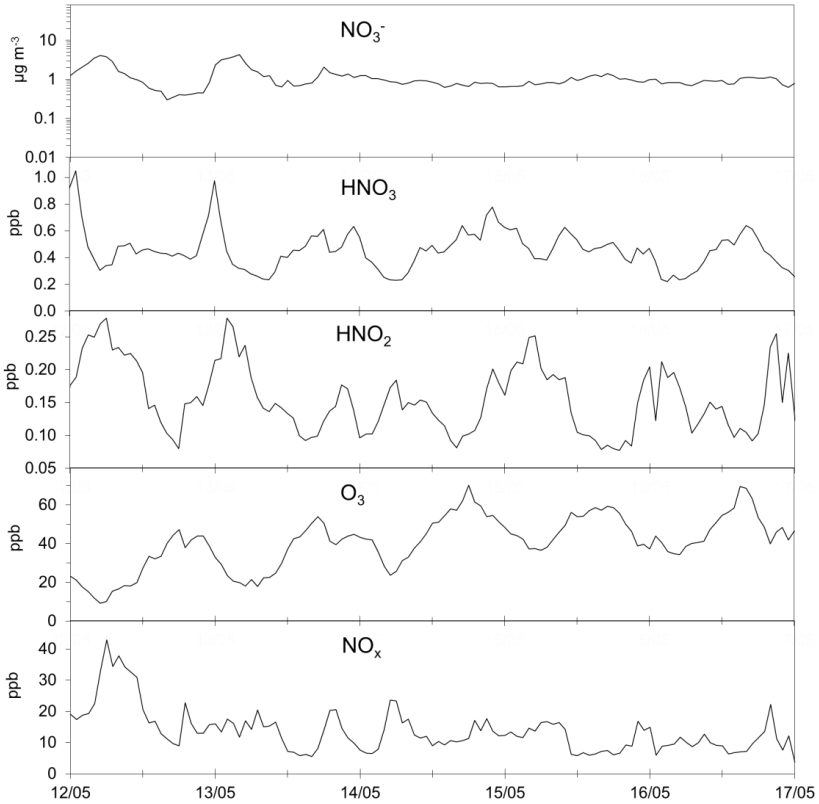

Fig. 8. Ozone, NO_x, and the nitrogen-containing gas-phase acids and nitrate in PM_{10} in late spring.

ACPD
12, 4755–4796, 2012

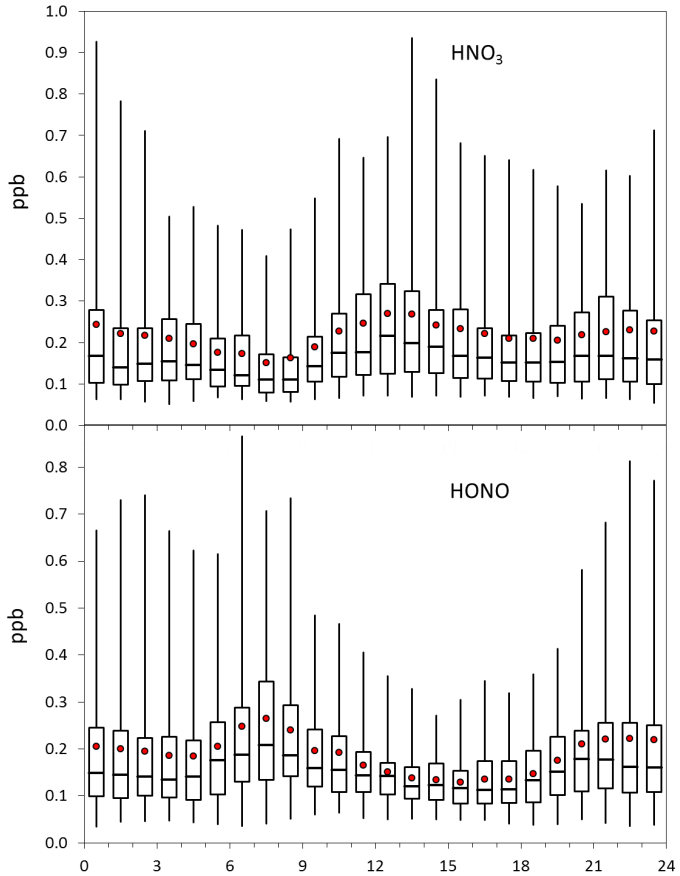

Fig. 9. Diurnal cycle of nitric and nitrous acids in March–May 2010. The box represents the 25th to 75th percentile range, the bars the 95 percent range (2.5th and 97.5th percentiles), the horizontal line the median and the red circle the averages of the hourly-averaged data of each hour.

ACPD
12, 4755–4796, 2012

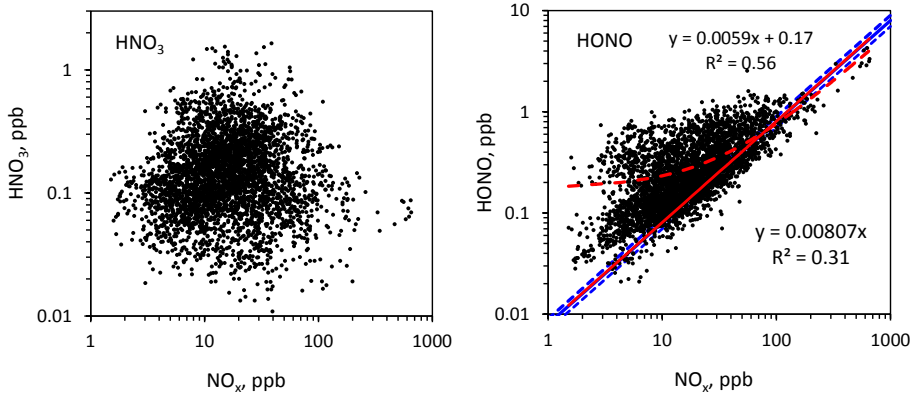

Fig. 10. Nitric and nitrous acid as a function of NO_x. The blue lines in the right panel are the HONO-to-NO_x ratios 0.008 ± 0.001 by Kurtenbach et al. (2001), the red continuous line the regression line that was done by forcing the offset to zero and the red dashed line without forcing the offset.

ACPD
12, 4755–4796, 2012

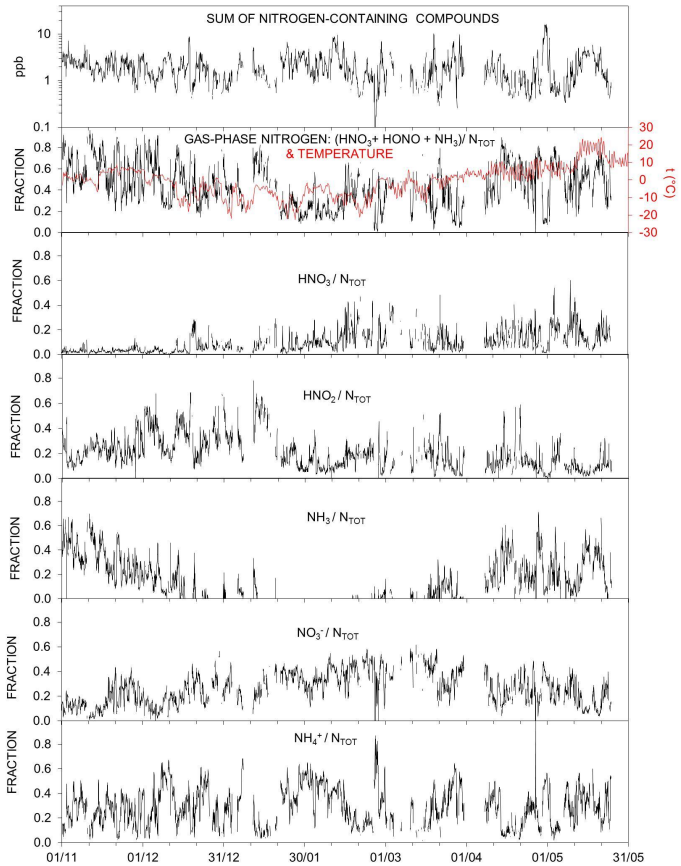

Fig. 11. Nitrogen fractionation into aerosol and gas phases. Upper panel: Sum of nitrogen-containing gases measurable with the MARGA (HNO_3 + HNO_2 + NH_3) and aerosols in PM_{10} (NO_3^- + NH_4^+) all in ppb. The panels below that: fractions of nitrogen-containing compounds of the sum of all of them.

ACPD
12, 4755–4796, 2012

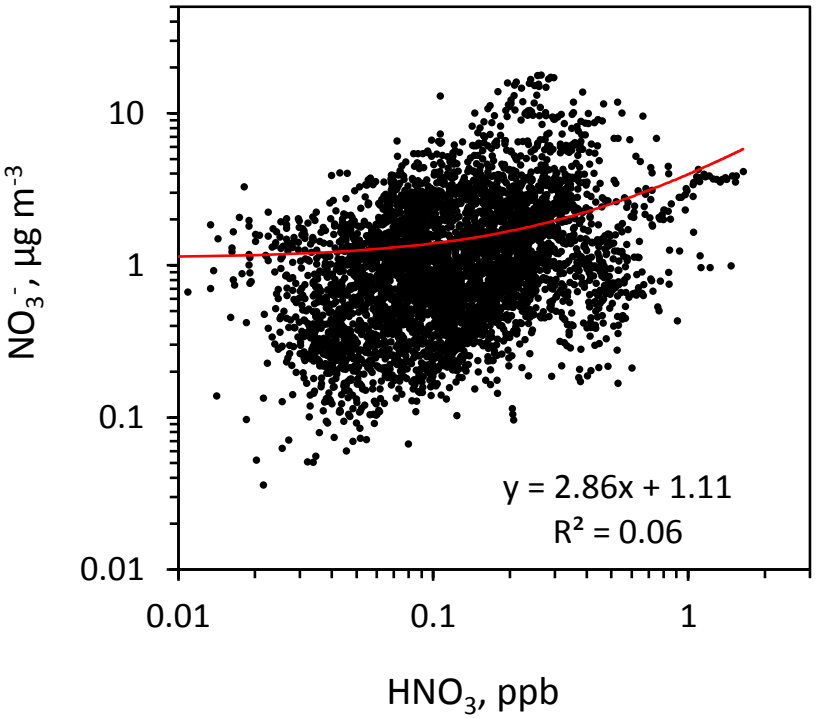

Fig. 12. Relationship of nitrate and nitric acid.

ACPD
12, 4755–4796, 2012

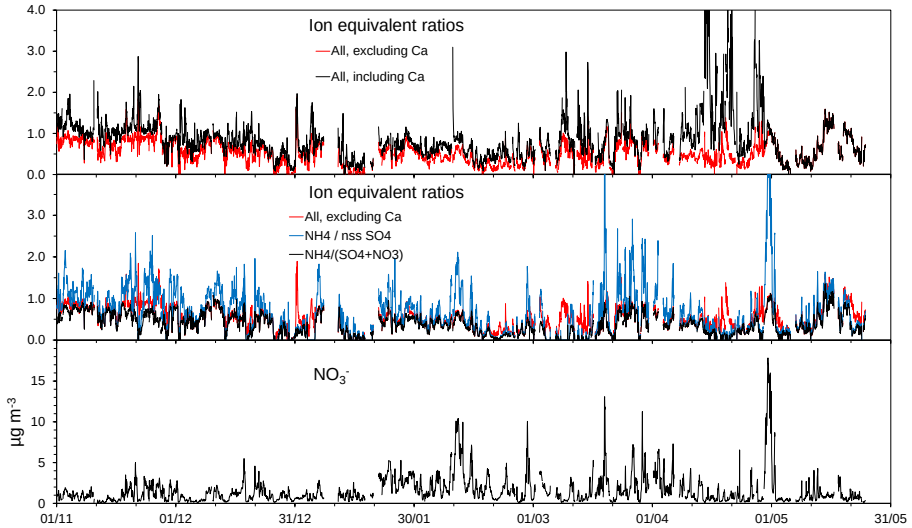

Fig. 13. Studies on the acidity of aerosols in PM_{10}. Upper panel: ratio of sums of ion equivalent concentrations of cations to that of anions, including and excluding Ca^{2+} concentrations; middle panel: ratio of sums of ion equivalent concentrations of cations to that of anions excluding Ca^{2+} concentrations, the ratio of ammonium to non-seasalt sulfate ion equivalent concentrations, and the ratio of ammonium to the sum of non-seasalt sulfate and nitrate ion equivalent concentrations; lower panel: nitrate concentrations.

ACPD
12, 4755–4796, 2012

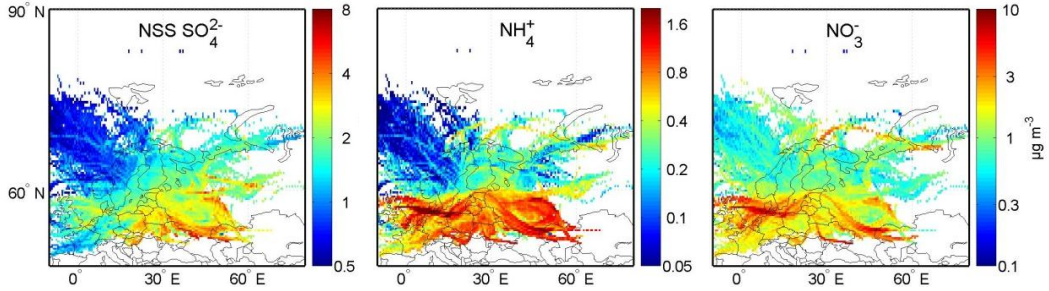

Fig. 14. Source areas of the most important secondary aerosol ion compounds as determined from trajectory statistics.

ACPD
12, 4755–4796, 2012

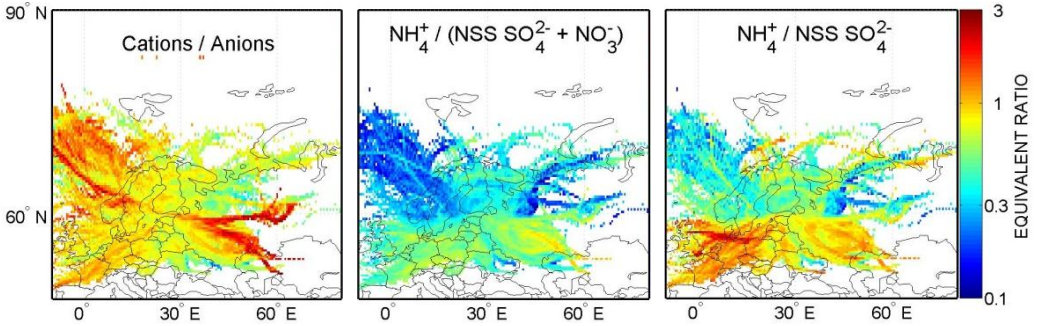

Fig. 15. Trajectory statistics of the ion equivalent ratios presented in Fig. 13.

ACPD
12, 4755–4796, 2012